Journal of Materials Chemistry A

Accepted Manuscript

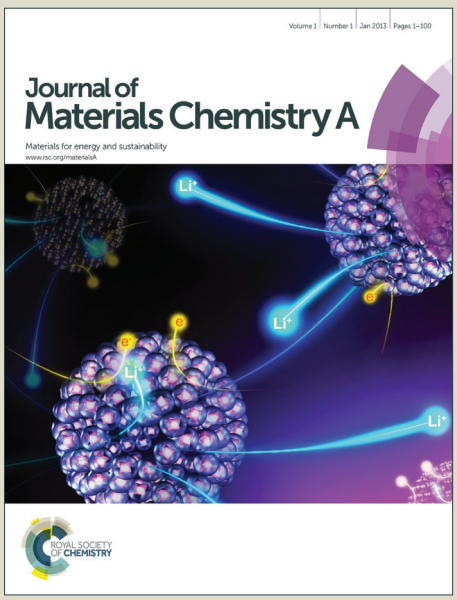

ROYAL SOCIETY OF CHEMISTRY

www.rsc.org/materialsA

Cite this: DOI: 10.1039/c0xx00000x

www.rsc.org/xxxxxx

ARTICLE TYPE

Photocatalytic Performance Enhanced via P3HT-g-C_3N_4 Heterojunction

Xiaojuan Bai[a, b], Changpo Sun[b], Songling Wu[b], Yongfa Zhu[a]*

Received (in XXX, XXX) Xth XXXXXXXXX 20XX, Accepted Xth XXXXXXXXX 20XX
DOI: 10.1039/b000000x

ABSTRACT: P3HT-g-C_3N_4 photocatalysts with high activity have been fabricated by assembling p-type P3HT particles on n-type g-C_3N_4 nanoplates via ball milling method. The photocatalytic activity of the P3HT-g-C_3N_4 photocatalysts for the degradation of MB was 2 times higher than that of pure g-C_3N_4. The formation of heterojunction interface of P3HT-g-C_3N_4 photocatalysts enhanced the separation efficiency of photogenerated electron-holes and resulted in the enhancement of photocatalytic performance. The potential difference in the heterojunction is the main driving force for efficient charge separation and transfer.

Introduction

Composites of carbon nanomaterials and conjugated polymers have been used extensively as active materials in environmental purification, organic photosynthesis, solar energy conversion and sustainable hydrogen production.[1] In principle, heterogeneous photocatalysis involves the generation, migration, and separation of charge carriers in light-excited semiconductors, in which the adsorbed substrates undergo redox reactions with the separated electrons and holes.[2,3] Metal-free polymeric semiconductors have recently been introduced as solar energy transducers and have gained great attentions. However, the photocatalytic systems developed thus far have been restricted by low efficiency, mainly because of the fast recombination of photoinduced electron-hole pairs.[4,5] The creation of tight junctions between two semiconductors not only depends on the electronic structure of the semiconductors but also on material properties, such as electron affinity and work function.[3,6] Several kinds of photocatalytic heterojunctions have been developed by coupling different types of photocatalysts. For example, the combination of p-type or n-type semiconductors has been reported to create p-n and n-n photocatalytic systems.[7-10] Recently, a binary carbon nitride (g-C_3N_4) based on s-triazine networks as a metal-free n-type photocatalysts for hydrogen production and environmental purification has been introduced.[1,11-13] Poly-3-hexylthiophene (P3HT) has proven thus far to be one of the best choices for p-type donor material in bulk heterojunction, and its use in conjunction with g-C_3N_4 as the n-type acceptor material is considered a natural combination due to very good hole and electron motilities in the two materials, respectively, [14] and the potentially ideal nanostructure of their distributed heterojunction provided effective phase separation at the nanoscale. P3HT is a p-type semiconductor with a band gap of 1.9-2.1 eV, higher holes carrier mobility (10^{-4}~10^{-3} cm^2/Vs), dissolubility, process ability and long-term stability.[15,16] As illustrated in Figure S1, once g-C_3N_4 and P3HT are integrated together, the band alignment between the two materials results in the formation of Type-II heterojunction. The redistribution of electrons and holes between g-C_3N_4 and P3HT may greatly reduce the energy-wasteful e^--h^+ recombination, and thus improving the photocatalytic activity. In principle it should be possible to realize that the successful separation and the prolonged lifetime of e^--h^+ pairs is beneficial for photocatalysis (Figure S2).

Although the previous works provided important insight into their electrical, optical, and structural properties of P3HT-g-C_3N_4 blends,[16] structure-activity relationship of P3HT-g-C_3N_4 composites can only be understand based on their activity trend and interface electronic structure at the molecular scale. This work suggests that two main factors contribute to the efficiency of charge transfer at the interface: the formation of a type-II heterojunction in the built-in field favors effective charge transfer ("electronic" factor), and the structure of the donor molecules at the interface, where the extended conjugation favors charge transfer analogous to the effect of crystalline regions in bulk polymers ("structural" factor). For g-C_3N_4 molecular structure, there are some docking sites containing -NH_2 and -NH- groups on the surface which formed through thermal condensation, this may be modified by many methods in polymer processing and chemistry field.[17,18]

In this work, P3HT-g-C_3N_4 photocatalysts were fabricated by ball milling method which is an effective way to synthesize materials in polymer processing and chemistry field. Since the π-conjugated effect of the polymer plays a crucial role in the charge transfer, we combined the Raman spectra with FTIR method to investigate the nature of self-assembly π-conjugation and its impact on the photocatalysis of P3HT-g-C_3N_4. The varying relative concentrations of P3HT/g-C_3N_4 are investigated and π-conjugated effect is elucidated systematically. This work demonstrated that the photocatalytic activity of P3HT-g-C_3N_4 for degradation of MB was 2 times higher than that of pure g-C_3N_4 and physical mixture of P3HT/C_3N_4 sample, which could be ascribed to the high separation efficiency of photogenerated

electrons and holes across the heterojunction interface of P3HT-g-C_3N_4 photocatalysts.

Experimental Section

Materials

P3HT sample was supported by J&K Scientific Ltd and the average molecular weight is 30000. Dicyandiamide was purchased from Sinopharm Chemical Reagent Corp, P. R. China. All other reagents used in this research were analytically pure and used without further purification. The bulk C_3N_4 photocatalysts were synthesized as described in a previous paper.[16] Dicyandiamide (3 g) (Aldrich, 99%) in an open crucible was heated in static air with a ramping rate of 2.3°C/min to 550°C where it was held for 4 h. The product was collected and ground into powder in an agate mortar for further characterization and performance measurements. It should be claimed that the widely used "g-C_3N_4" in the literature is actually nonstoichiometric. Here we use "g-C_3N_4" to describe the products just to keep consistent with the general usage.

Synthesis of P3HT-g-C_3N_4 samples

The typical P3HT-g-C_3N_4 composite photocatalysts were prepared as follows: The bulk g-C_3N_4 was added with different amount of P3HT and then was ball milled for certain times resulting in ultrafine burgundy powder (300 rps). The product was collected for further characterization and performance measurements. With different P3HT amount loaded on g-C_3N_4, the color of final products is different, which changes from light-burgundy to deep-burgundy. The P3HT-g-C_3N_4 photocatalysts with different P3HT ratio from 0.2 wt.% to 5.0 wt.% were prepared according to above method. As a reference, the 0.7 wt.% of mixture P3HT/C_3N_4 was prepared by finely grinding a certain amount of bulk g-C_3N_4 and P3HT, then stirred mechanically at low speed and energy to form uniform P3HT/C_3N_4 mixture. The annealed composite was obtained through the composite 0.7 wt.% P3HT-g-C_3N_4 was calcined at 120°C for 4 h, which was due to the optimum holes mobility of P3HT can achieve for 10^{-3} cm^2/Vs at 120 °C.

The g-C_3N_4 and P3HT-g-C_3N_4 electrodes were prepared as follows: 4 mg of as-prepared photocatalyst was suspended in 2 mL water to produce slurry, which was then dip-coated onto a 2 cm × 4 cm indium-tin oxide (ITO) glass electrode. Electrodes were exposed to UV light for 10 h to eliminate ethanol and subsequently calcined at 200 °C for 8 h under N_2 flow (rate = 60 ml/min). All investigated electrodes were of similar thickness (0.8-1.0 μm).

Characterizations

Transmission electron microscopy (TEM) images were obtained by JEOL JEM-2011F field emission transmission electron microscope with an accelerating voltage of 200 kV. To avoid electron beam-induced damage, low-intensity beam was used for collecting selected area electron diffraction (SAED) patterns. X-ray diffraction (XRD) patterns of the powders were recorded at room temperature by a Bruker D8 Advance X-ray diffractometer. The diffuse reflectance absorption spectra (DRS) of the samples were recorded in the range from 250 to 800 nm using a Hitachi U-3010 spectroscope equipped with an integrated sphere attachment and $BaSO_4$ was used as a reference. Raman spectra were recorded on a microscopic confocal Raman spectrometer (Renishaw 1000 NR) with an excitation of 514.5 nm laser light. The room-temperature photoluminescence (PL) spectra of g-C_3N_4 and P3HT-g-C_3N_4 samples were investigated utilizing the Perkin-Elmer LS55 spectrophotometer equipped with xenon (Xe) lamp with an excitation wavelength of 370 nm. Fourier transform infrared (FTIR) spectra were carried out using Perkin-Elmer spectrometer in the frequency range of 4000-450 cm^{-1} with a resolution of 4 cm^{-1}. X-ray photoelectron spectroscopy (XPS) was measured in a PHI 5300 ESCA system. The beam voltage was 3.0 kV, and the energy of Ar ion beam was 1.0 keV. The binding energies were normalized to the signal for adventitious carbon at 284.8 eV. Electrochemical and photoelectrochemical measurements were performed in a three electrode quartz cells with 0.1M Na_2SO_4 electrolyte solution. Platinum wire was used as counter and saturated calomel electrode (SCE) used as reference electrodes, respectively. And g-C_3N_4 and P3HT-g-C_3N_4 film electrodes on ITO served as the working electrode. The photoelectrochemical experiment results were recorded with an electrochemical system (CHI-660B, China). The visible irradiation was obtained from a 500 W Xe lamp (Institute for Electric Light Sources, Beijing) with a 420 nm cut-off filter. Potentials are given with reference to the SCE. The photoresponses of the photocatalysts as visible light on and off were measured at 0.0V.

Photocatalytic Experiments

The photocatalytic activities were evaluated by the decomposition of methylene blue (MB) and phenol under visible light irradiation (λ > 420 nm). Visible irradiation was obtained from a 500 W Xe lamp (Institute for Electric Light Sources, Beijing) with a 420 nm cutoff filter, and the average visible light intensity was 38 mW/cm^2. 25 mg of photocatalyst was totally dispersed in an aqueous solution of MB (50 mL, 0.03 mM) or phenol (50 mL, 5 ppm). Before irradiation, the suspensions were magnetically stirred in dark for 60 min to get absorption-desorption equilibrium between the photocatalyst and MB (phenol). At certain time intervals, 3 mL aliquots were sampled and centrifuged to remove the particles. The concentration of MB was analyzed by recording the absorbance at the characteristic band of 663 nm using a Hitachi U-3010 UV-Vis spectrophotometer and phenol was detected using a HPLC method with a UV detector at 270 nm. To investigate the active species generated in the photocatalytic degradation process, the experiments of free radicals (hydroxyl radical (·OH), hole (h^+), superoxide radical capture were carried out by tertbutylalcohol (*t*BuOH), ethylenediamine tetraacetic acid disodium salt (EDTA-2Na) and benzoquinone, respectively.

Results and Discussion

Morphology of P3HT-g-C_3N_4 Photocatalysts

The successful formation of the P3HT-g-C_3N_4 heterostructure is clearly demonstrated by the TEM images in Figure 1. The thin layers and regular sphere are identified for g-C_3N_4 and P3HT (Figure 1a and insert image), respectively. As shown in Figure 1b, g-C_3N_4 sample is found packing closely onto P3HT surface and exhibit dense thick sheets, both of which are integrated

together as a p-n heterojunction, resulting in the P3HT-g-C_3N_4 hybrid. The result revealed that P3HT adsorbs strongly to the g-C_3N_4 through stacking forces which formed ranging from lamellar assemblies to more disordered, bundled conformations. The two phases of g-C_3N_4 and P3HT can be observed carefully and closely contact to form an intimate interface. According to the previous reports and our experiment results,[19-21] (Figure S3) the two-dimensional ordering of g-C_3N_4 and P3HT is very weak and it is hard to find the clear lattice fringe of g-C_3N_4 and P3HT from the high-resolution TEM image, which was attributed to the indistinct in-plane diffraction (100) in XRD pattern.

These P3HT-g-C_3N_4 p-n heterostructures were further characterized by the high-resolution X-ray photoelectron spectroscopy (XPS) spectra of S2p and C1s. In Figure 1c, two

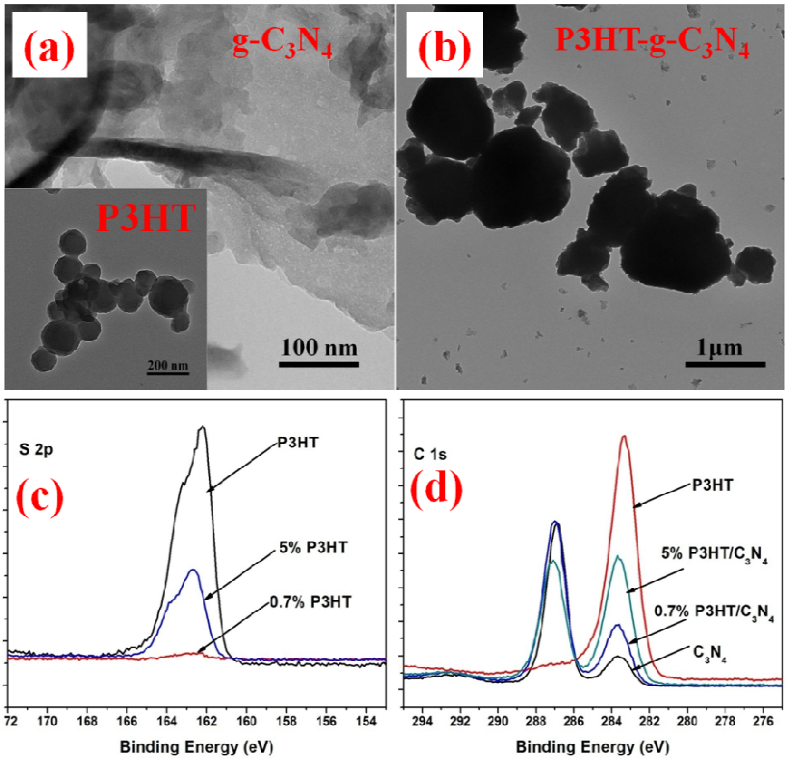

Figure 1. (a) TEM images of g-C_3N_4 and P3HT (insert) semconductor. (b) TEM image of P3HT-g-C_3N_4 polymer composite. (c) High-resolution XPS spectra of S2p recorded from P3HT, g-C_3N_4 and P3HT-g-C_3N_4. (d) High-resolution XPS spectra of C1s.

independent binding energy (BE) peaks of S2p centering at 162.7 eV and 163.8 eV are found for P3HT-g-C_3N_4, but are absent for the pristine g-C_3N_4. These BE values are close to those of the pristine P3HT (162.2 eV and 163.2 eV). Thus, the S2p spectra of P3HT-g-C_3N_4 further confirms the formation of P3HT-g-C_3N_4 heterostructures. In addition, as shown in Figure 1d, the BEs of C1s for P3HT-g-C_3N_4 (283.7 eV and 287.0 eV) are quite different from pristine g-C_3N_4 (283.6 eV and 286.8 eV), illustrating that the grafted P3HT is modified to the g-C_3N_4, rather than providing a sulfur source for doping the g-C_3N_4 matrix by treatment of ball milling at high energy. As shown in Figure S4, the N1s intensity of P3HT-g-C_3N_4 composites shows the opposite tendency relative to S2p and C1s, and the peak C-N-C (398.8 eV) shifts slightly to the higher binding energy, illustrating that the P3HT nanospheres were wrapped chemically by g-C_3N_4 nanoplates.

Enhancement of Photocatalytic Activity

The rate of photodegradation for MB on P3HT-g-C_3N_4 photocatalysts with different amounts of P3HT is shown in Figure 2a and Figure 2b. With an increase in the amount of P3HT and the extended time, the rate of photodegradation of MB increases firstly and then achieves a maximum when the amount of P3HT is about 0.7 wt % for 4 h by treatment of ball milling. The apparent reaction rate is estimated to be as high as 0.18134 h^{-1} and the activity is increased by up to 2 times for high concentration of MB after adding 0.7 wt% P3HT to g-C_3N_4. However, the rate of photodegradation of MB decreases when the amount of P3HT is higher than 0.7 wt%. The density of P3HT nanospheres wrapped by g-C_3N_4 nanoplates increases step-by-step with the enhancement of P3HT content. In the case of 0.7 wt% P3HT-g-C_3N_4 heterojunction, the surface of P3HT has been covered by g-C_3N_4 nanoplates well. However, further increase of P3HT content results in a drastic overlapping of P3HT nanosphere, which is helpless for fabrication of heterojunction with a close interface. Only the tight coupling is favorable for the charge transfer between g-C_3N_4 and P3HT and promotes the separation of photogenerated electron-hole pairs, subsequently improving the photocatalytic activity. The P3HT-g-C_3N_4 sample also shows obvious higher photocatalytic activity for the decomposition of phenol than pristine g-C_3N_4 (Figure 2c). After being annealed treatment, the photodegradation rate of P3HT-g-C_3N_4 decreases slightly, which may be induced by the changed of molecular arrangement during the annealing process (Figure 2d). Figure S5 illustrates the relationship between degradation ratio of MB and cycle times. After reusing four cycles about 20 h, the

photodecomposition rate of 0.7 wt.% P3HT-g-C_3N_4 for MB still remains over 80%.

Structure of Heterojunction Photocatalyst

The UV-visible diffuse reflectance spectra (DRS) show that the onset of the absorption edge of g-C_3N_4 is at 450 nm, corresponding to the band gap of 2.75 eV (shown in Figure 3a). Furthermore, the absorption intensity of the P3HT-g-C_3N_4 composites increases remarkably with an increase in the amount

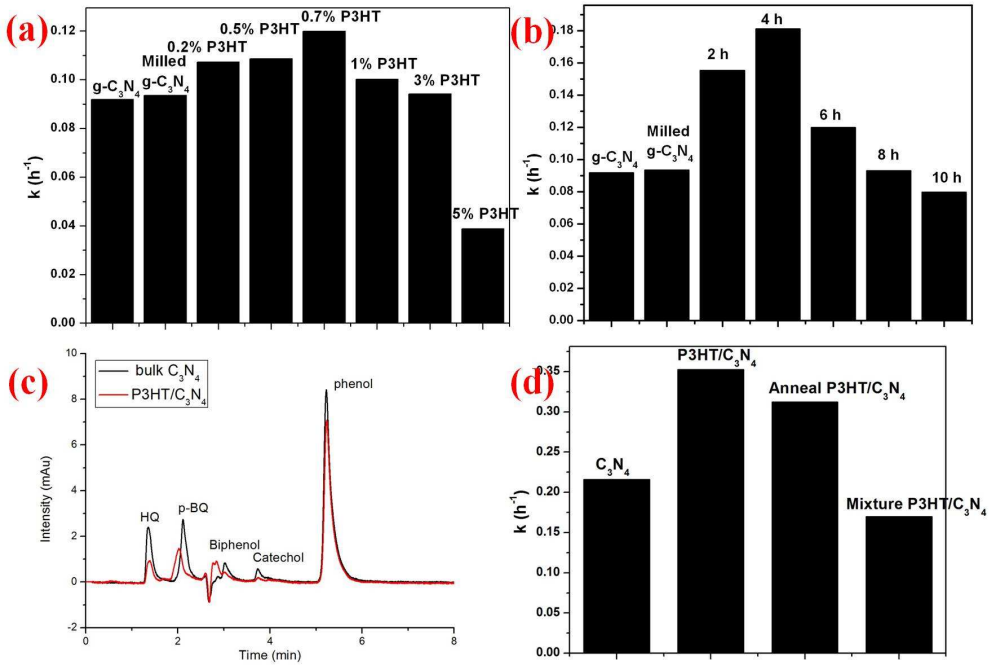

Figure 2. (a) Apparent rate constants for the photocatalytic degradation of MB over P3HT-g-C_3N_4 composite with different amount of P3HT. (b) The rate for the degradation of MB over P3HT-g-C_3N_4 composite for different ball-milling time. (c) The rate for the degradation of phenol. (d) The rate for MB degradation of mixture and annealed product. (Visible light: $\lambda > 420$ nm, [MB] = 0.03 mM, [phenol] = 5 ppm)

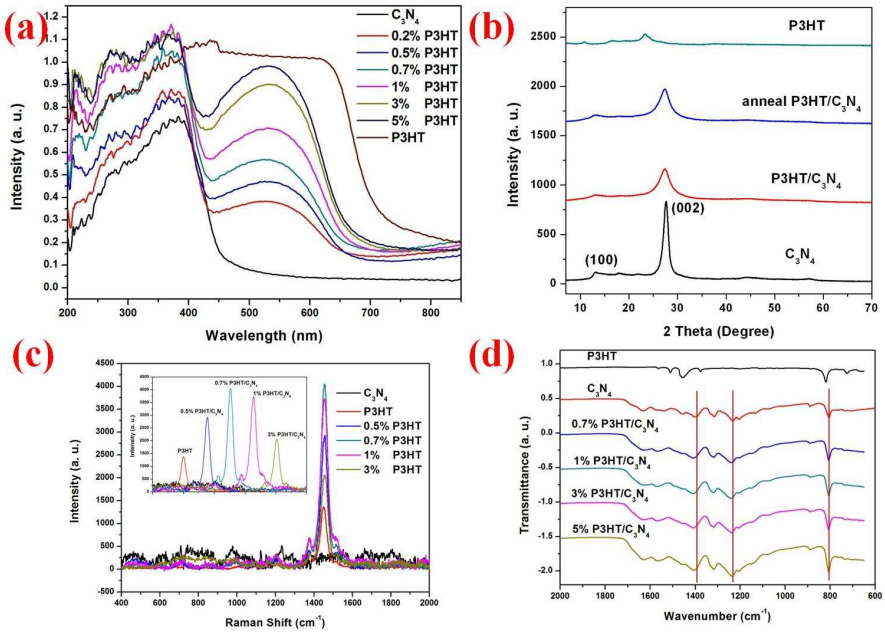

Figure 3 (a) DRS of P3HT-g-C_3N_4 polymer composite (b) XRD patterns of P3HT-g-C_3N_4 polymer composite (c) Raman spectrum of P3HT-g-C_3N_4 composite under 514 nm excitation. (d) FT-IR spectrum of P3HT-g-C_3N_4 composite.

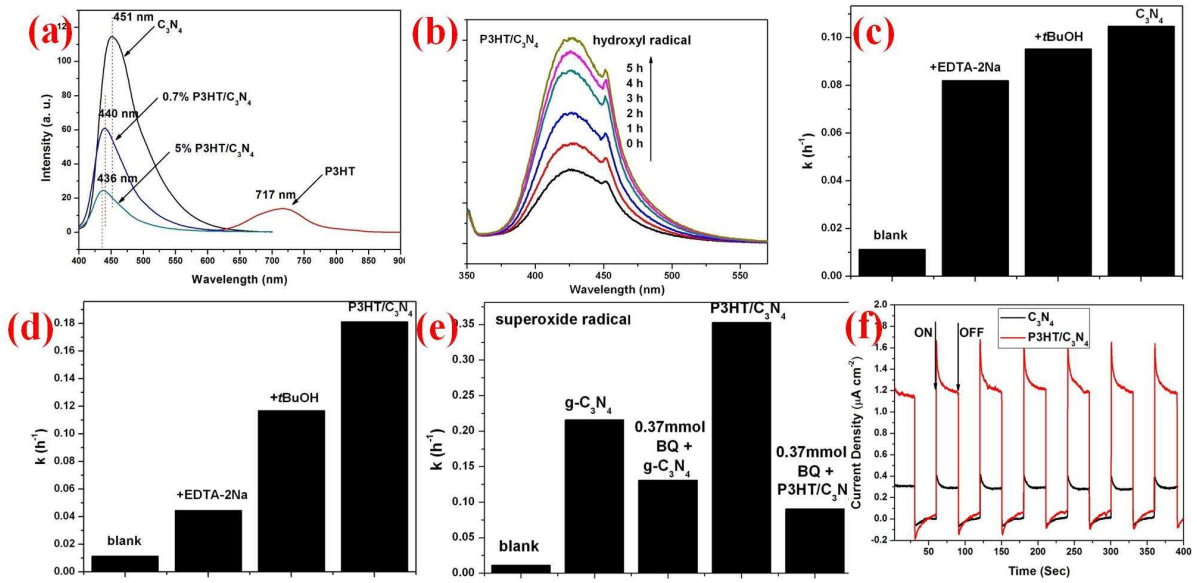

Figure 4. (a) PL spectra of P3HT-g-C_3N_4 polymer composite under 370 nm excitation at 298 K. (b) The changes in the fluorescence spectra of the irradiated P3HT-g-C_3N_4 (0.5 g L^{-1}) suspension containing 4 mM disodium terephthalate after various irradiation periods. (c) The rate for the degradation of MB over g-C_3N_4 with the additon of holes and hydroxyl radical scavenger. (d) The rate for the degradation of MB over P3HT-g-C_3N_4 composite with the additon of scavengers. (e) The rate for the degradation of MB with the additon of superoxide radical scavenger over g-C_3N_4 and P3HT-g-C_3N_4. (f) The photocurrent generation at g-C_3N_4 and P3HT-g-C_3N_4 electrodes in 0.1M Na_2SO_4 aqueous solution without any bias potential.

of P3HT, and its edge could shift to 704 nm. Note that the physical mixture of P3HT and g-C_3N_4 failed to produce close interconnection between P3HT and g-C_3N_4 (in Figure S6). X-ray diffraction patterns (XRD) from the samples, shown in Figure 3b, indicate that coupling C_3N_4 with P3HT can form intimate interfaces between C_3N_4 and P3HT in P3HT-g-C_3N_4 heterojunction, rather than form loose interfaces in the mechanically mixed sample. Raman spectroscopy is a simple, widely used technique to study vibrational modes of molecules. This technique together with quantum chemical calculations of Raman modes can provide an important insight into the fundamental structure-property relationships of molecular materials.[22-24] Figure 3c shows a typical Raman spectrum of g-C_3N_4, P3HT and P3HT-g-C_3N_4 samples excited at 514 nm. g-C_3N_4 shows weak Raman signal but there are various Raman modes at 400-2000 cm^{-1} for P3HT and P3HT-g-C_3N_4 samples: the main in-plane ring skeleton modes at ~1455 cm^{-1} (symmetric C=C stretch mode) and at ~1376 cm^{-1} (C-C intraring stretch mode), the interring C-C stretch mode at ~1208 cm^{-1}, the C-H bending mode with the C-C interring stretch mode at ~1180 cm^{-1}, and the C-S-C deformation mode at 728 cm^{-1}.[25,26] Among these Raman modes, we focus on the two main in-plane ring skeleton modes at ~1455 and ~1376 cm^{-1}, as they are supposed to be sensitive to π-electron delocalization (conjugation length) of P3HT molecules.[27] The Raman intensity of the C=C mode for P3HT-g-C_3N_4 (0.7 wt.%) under 514 nm excitation is increased approximately 3-fold in compared with pristine P3HT, which induces by a preresonant Raman effect leading to an increase in the intensity of the Raman peaks, indicating more ordered and longer conjugated segments exist in the P3HT-g-C_3N_4 system. According to the previous report, for P3HT, the intensity of the C-C mode relative to the C=C mode ($I_{C-C}/I_{C=C}$) decreases with decreasing chain length, without significant changes in the peak position.[28] This result suggests that a molecule with a shorter conjugation segment has a smaller relative C-C mode intensity as compared to a molecule with a longer conjugation segment. For P3HT-g-C_3N_4 system, a shorter conjugation segment of P3HT means a more widely conjugated system between P3HT and g-C_3N_4 is formed. It is worth noting that an interesting trend of the Raman intensity and photocatalysis in P3HT-g-C_3N_4 system. The trend of such a change of the C=C mode peak intensity is consistent with the photocatalytic activity. The relationship between them may be attributed to a longer conjugated length with planar chain conformation than that of pristine g-C_3N_4, which is consistent with a higher degree of molecular ordering in P3HT-g-C_3N_4. This high degree of molecular order can lead to an increase in absorption at longer wavelength and a dramatic increase in holes carrier mobility as compared to its disordered form.[29-31] Therefore, the degree of molecular order of P3HT-g-C_3N_4 in the systems is well correlated with the performance of the photocatalytic activity. FTIR spectra is shown in Figure 3d, the band at 1392 cm^{-1} of P3HT-g-C_3N_4 which be attributed to characteristic vibrational of g-C_3N_4 shifted toward short wavelength (1407 cm^{-1}), suggesting the chemical bonding effect in π-conjugated system between P3HT and g-C_3N_4 is reinforced.

Mechanism on Enhancement of Photocatalytic Activity

Photoluminescence (PL) spectra originating from the recombination of free charge carriers, usually serve as a good candidate for the characterization of heterostructures, indicating the process of charge migration, transfer and separation.[3,32,33] In Figure 4a, a strong PL emission peak centered at 451 nm is observed for the pristine g-C_3N_4, attributed to the radiative recombination of charge carriers. This energy-wasteful process can be greatly suppressed in P3HT-g-C_3N_4 with the localization

of electrons in one side g-C_3N_4 and holes in the other side P3HT by the band offsets. The formation rate of •OH at the photo-illuminated sample-water interface could also be detected by the PL technique using TA (terephthalic acid) as a probe molecule (in Figure 4b). The amount of •OH produced in the photo-irradiated P3HT-g-C_3N_4 suspension was estimated by measuring the amount of TAOH, which was generated by the reaction of •OH with TA. The fluorescence intensity increases with irradiation time under visible light irradiation. Thus, the intrinsic drawbacks of fast charge recombination in polymeric P3HT-g-C_3N_4 photocatalysts have been addressed by the construction of heterostructures, and a better photocatalytic performance has been realized. The BET surface area (S_{BET}) of the pure g-C_3N_4 and 5.0 wt.% composites was 15.8 and 4.8 m^2 g^{-1} respectively, while that of 0.7 wt.% composites was 3.8 m^2 g^{-1}, which is lower than pure g-C_3N_4 and 5.0 wt.% composites (Figure S7). This result demonstrated that the S_{BET} of the P3HT-g-C_3N_4 composite catalysts decreased with the addition of P3HT, indicating that the specific surface area does not contribute to photocatalytic activity of composite photocatalysts.

To further confirm the mechanism, the trapping experiments of radicals were performed using *t*-BuOH as hydroxyl radical scavenger,[34] EDTA-2Na as holes radical scavenger[35] and benzoquinone as superoxide radical scavenger.[36] As shown in Figure 4c, Figure 4d and Figure 4e, the photocatalytic activity of P3HT-g-C_3N_4 samples reduced largely accordingly, while activity of g-C_3N_4 decreases slightly by the addition of holes capture and superoxide radical scavenger, indicating that holes and superoxide radical are the main oxidative species for P3HT-g-C_3N_4 samples, which induced by high holes carrier mobility of longer conjugation segment of P3HT-g-C_3N_4. The photocurrent generation by the heterostructure was examined without any bias potential (Figure 4f). Upon visible light irradiation, a fast and stable photocurrent was produced, indicating the generation and separation of photoinduced e^--h^+ pairs at sample/water interfaces. As expected, an overall enhanced photocurrent is obtained on P3HT-g-C_3N_4, which may attributed to the improved efficiency of charge separation and the prolonged lifetime of charge carriers involved in photoredox reaction.

In summary, while g-C_3N_4 was hybridized by P3HT, a p-n heterojunction would be formed and the charge carriers would diffuse in opposite direction to form an internal electric field with a direction from n-type g-C_3N_4 to p-type P3HT at the heterojunction interface. P3HT and g-C_3N_4 could be simultaneously excited to generate electron-hole pairs. According to the band edge position, the excited electrons produced by P3HT were injected into the CB of g-C_3N_4, while the photogenerated holes were effectively collected in the VB of P3HT. Because of the formation of internal electricfield, the migration of photogenerated carriers was promoted. Therefore, the photogenerated carriers could be effectively separated, resulting in higher photocatalytic performance.

Conclusions

P3HT-g-C_3N_4 heterojunctions were prepared by blend method based on band alignment Type-II p-n junction between P3HT and g-C_3N_4. The enhancement of photocatalytic activity could be ascribed to formation of internal electricfield induced the enhanced separation efficiency of photogenerated electrons and holes. P3HT plays an important role of increasing the π-conjugation length in the system, which is an effect deriving from the π-π stacking interaction at the interface between p-type P3HT donor and n-type g-C_3N_4 acceptor systems. This work could open possibilities for improved preparation and activity of photocatalytic materials based on π-conjugated polymer in general.

Supporting Information

The part included schematic illustration of organic heterojunction, charge separation and photocatalytic process, DRS of P3HT-g-C_3N_4 composite. This material is available free of charge via the Internet or from author.

Acknowledgment

This work was partly supported by National Basic Research Program of China (973 Program (2013CB632403) National High Technology Research and Development Program of China (2012AA062701) and Chinese National Science Foundation (20925725and 21373121).

Notes and references

[a]Department of Chemistry, Beijing Key Laboratory for Analytical Methods and Instrumentation, Tsinghua University, Beijing, China 100084
[b]Academy of State Administration of Grain, No. 11 Baiwanzhuang Street, Beijing, 100037, China.

†Electronic Supplementary Information (ESI) available: [schematic illustration of organic heterojunction, charge separation and photocatalytic process, TEM, XPS, BET, DRS and cycle experimental data of P3HT-g-C_3N_4 composite]. See DOI: 10.1039/b000000x/

1. X. C. Wang, K. Maeda, A. Thomas, K. Takanabe, G. Xin, K. Domen, M. Antonietti, *Nat. Mater*. 2009, **8**, 76.
2. K. Maeda, A. Xiong, T. Yoshinaga, T. Ikeda, N. Sakamoto, T. Hisatomi, M. Takashima, D. Lu, M. Kanehara, T. Setoyama, T. Teranishi, K. Domen, *Angew. Chem. Int. Ed*. 2010, **49**, 4096.
3. J. S. Zhang, M. W. Zhang, R. Q. Sun, X. C. Wang, *Angew. Chem.* 2012, **124**, 10292.
4. M. Schwab, M. Hamburger, X. Feng, J. Shu, H. Spiess, X. Wang, M. Antonietti, K. Mullen, *Chem. Commun*. 2010, **46**, 8932.
5. K. Maeda, K. Domen, *J. Phys. Chem. Lett.* 2010, **1**, 2655.
6. J. Tersoff, *Phys. Rev. B* 1984, **30**, 4874.
7. G. Li, K. A. Gray, *Chemical Physics*. 2007, **339**, 173.
8. H. G. Kim, P. H. Borse, J. S. Jang, E. D. Jeong, J. S. Lee, *Materials Letters*. 2008, **62**, 1427.
9. X. P. Lin, J. C. Xing, W. D. Wang, Z. C. Shan, F. F. Xu, F. Q. Huang. *J. Phys. Chem. C* 2007, **111**, 18288.
10. O. Khaselev, J. A. Turner, *Science*. 1998, **280**, 425.
11. X. Wang, K. Maeda, X. Chen, K. Takanabe, K. Domen, Y. Hou, X. Fu, M. Antonietti, *J. Am. Chem. Soc.* 2009, **131**, 1680.
12. J. Zhang, M. Grzelczak, Y. Hou, K. Maeda, K. Domen, X. Fu, M. Antonietti, X. Wang, *Chem. Sci.* 2012, **3** , 443
13. X. J. Bai, L. Wang, R. L. Zong, Y. F. Zhu, *J. Phys. Chem. C* 2013, **117**, 9952.
14. A. C. Mayer, S. R. Scully, B. E. Hardin, M. W. Rowell, M. D. McGehee, *Mater. Today* 2007, **10**, 28.
15. B. R. Saunders and M. L. Turner, *Adv. Colloid Interface Sci*. 2008, **138**, 1.
16. H. J. Yan, Y. Huang, *Chem. Commun*. 2011, **47**, 4168
17. J. Zhang, G. Zhang, X. Chen, S. Lin, L. Mohlmann, G. Dolega, G. Lipner, M. Antonietti, S. Blechert, X. Wang, *Angew. Chem.* 2012, **124**, 3237.
18. J. Zhang, M. Zhang, G. Zhang, X. Wang, *ACS Catal.* 2012, **2**, 940.

19. F. Dong, Z. W. Zhao, T. Xiong, Z. L. Ni, W. D. Zhang, Y. J. Sun, W. K. Ho. *ACS Appl. Mater. Interfaces* 2013, **5**, 11392.
20. Y. L. Tian, B. B. Chang, J. L. Lu, J. Fu, F. N. Xi, X. P. Dong. *ACS Appl. Mater. Interfaces* 2013, **5**, 7079.
21. X. J. Bai, R. L. Zong, C. X. Li, D. Liu, Y. F. Liu, Y. F. Zhu. *Applied Catalysis B: Environmental.* 2014, **147**, 82.
22. E. C. Honea, A. Ogura, C. A. Murray, K. Raghavachari, Wo. Sprenger, M. F. Jarrold, W. L. Brown, *Nature* 1993, **366**, 42.
23. C. L. Donley, J. Zaumseil, J. W. Andreasen, M. M. Nielsen, H. Sirringhaus, R. H. Friend, J. S. Kim, *J. Am. Chem. Soc.* 2005, **127**, 12890.
24. J. P. Schmidtke, J. S. Kim, J. Gierschner, C. Silva, R. H. Friend, *Phys. Rev. Lett*. 2007, **99**, 167401.
25. M. Baibarac, M. Lapkowski, A. Pron, S. Lefrant, I. Baltog, *J. Raman Spectrosc.*1998, **29**, 825.
26. A. M. Ballantyne, T. A. M. Ferenczi, M. Campoy-Quiles, T. M. Clarke, A. Maurano, K. H. Wong, W. M. Zhang, N. Stingelin-Stutzmann, J. S. Kim, D. D. C. Bradley, J. R. Durrant, I. McCulloch, M. Heeney, J. Nelson, S. Tierney, W. Duffy, C. Mueller, P. Smith, *Macromolecules*. 2010, **43**, 1169.
27. Y. Gao, J. K. Gery, *J. Am. Chem. Soc.* 2009, **131**, 9654.
28. W. C. Tsoi, D. T. James, J. S. Kim, P. G. Nicholson, C. E. Murphy, D. D. C. Bradley, J. Nelson, J. S. Kim. *J. Am. Chem. Soc.* 2011, **133**, 9834.
29. P. J. Brown, D. S. Thomas, A. Kohler, J. S. Wilson, J. S. Kim, C. M. Ramsdale, H. Sirringhaus, R. H. Friend, *Phys. Rev. B* 2003, **67**, 064203.
30. S. S. Pandey, W. Takashima, S. Nagamatsu, T. Endo, M. Rikukawa, K. Kaneto, *Jpn. J. Appl. Phys. Part 2*, 2000, **39**, L94.
31. H. Sirringhaus, P. J. Brown, R. H. Friend, M. M. Nielsen, K. Bechgaard, B. M. W. Langeveld-Voss, A. J. H. Spiering, R. A. J. Janssen, E. W. Meijer, P. Herwig, D. M. de Leeuw, *Nature*. 1999, **401**, 685.
32. X. Gao, W. Sun, Z. Hu, G. Ai, Y. Zhang, S. Feng, F. Li, L. Peng, *J. Phys. Chem. C*. 2009, **113**, 20481.
33. T. Kawahara, Y. Konishi, H. Tada, N. Tohge, J. Nishii, S. Ito, *Angew. Chem.* 2002, **114**, 2935.
34. H. Lee, W. Y. Choi, *Environ. Sci. Technol*. 2002, **36**, 3872.
35. J. H. Zhou, C. Y. Deng, S. H. Si, Y. Shi, X. L. Zhao, *Electrochimica Acta*. 2011, **56**, 2062.
36. W. Liu, M. L. Wang, C. X. Xu, S. F. Chen, *Chemical Engineering Journal*. 2012, **209**, 386.

For Table of Contents Use Only

Photocatalytic Performance Enhanced via P3HT-g-C_3N_4 Heterojunction

Xiaojuan Bai[a, b], *Changpo Sun*[b], *Songling Wu*[b], *Yongfa Zhu*[a]*

[a]Department of Chemistry, Beijing Key Laboratory for Analytical Methods and Instrumentation, Tsinghua University, Beijing, China, 100084

[b]Academy of State Administration of Grain, No. 11 Baiwanzhuang Street, Beijing, China, 100037.

Scheme1. Schematic illustration of charge separation and photocatalytic process over g-C_3N_4 and P3HT-g-C_3N_4 photocatalysts under visible light irradiation